DOI: 10.1021/ma100318j

Macromolecules
ARTICLE

Formation of Nanostructured Poly(dicyclopentadiene) Thermosets Using Reactive Block Polymers

Mark A. Amendt, Liang Chen, and Marc A. Hillmyer*

Department of Chemistry, University of Minnesota, Minneapolis, Minnesota 55455

Received February 8, 2010; Revised Manuscript Received March 10, 2010

ABSTRACT: Nanostructured thermosets were prepared by reaction-induced phase separation (RIPS) using a metathesis-cross-linkable monomer in the presence of a metathesis-reactive block polymer. Mixtures of poly(norbornenylethylstyrene-*s*-styrene)-*b*-poly(lactide) (PNS−PLA) and dicyclopentadiene (DCPD) in tetrahydrofuran were cross-linked using the second generation Grubbs catalyst. Small-angle X-ray scattering analysis of a series of cured films containing PNS−PLA with varied PLA block lengths and 0−83 wt % DCPD indicated the presence of nanophase-separated disordered morphologies postcuring in most cases. Scanning electron microscopy of cured films after removal of the PLA phase revealed that a majority of the films exhibited a bicontinuous structure. Mechanistic investigations demonstrated that cross-linking the PNS block into the matrix was vital in preventing macrophase separation, and the morphologies observed were relatively unaffected by variations in the concentration of the catalyst. We propose a general mechanism for the formation of nanostructured DCPD using this protocol and develop critical conditions for the formation of bicontinuous structures based on the extent of overlap of the block polymer.

Introduction

The formation of nanostructured ceramics, polymers, and composite materials has been at the forefront of numerous research endeavors. In particular, nanostructured thermosets have received attention as the thermal,[1] dielectric,[2] diffusion,[3] and mechanical[3,4] properties of these materials can be systematically tuned depending on the components incorporated. Thermosets are formed by the coupling reactions of multifunctional monomers into a network structure, and the nanostructuring of thermosets can be accomplished through the incorporation of an additive that is integrated into the final structure upon curing. Examples of such additives include nanoparticles,[1,2] liquid crystals,[3] nanotubes,[4] and block polymers.[5]

Block polymers self-assemble into nanometer-sized morphologies that minimize unfavorable contact between the chemically distinct monomers and avoid excessive stretching of the component blocks.[6] When incorporated into thermosetting systems, nanostructured materials can be formed. An early example of this was demonstrated by Hillmyer et al.[5] using an amphiphilic block polymer and an epoxy resin. Since that time, many examples of nanostructured epoxies using block polymers have been reported.[5,7−13] In most of these cases, the block polymer contains an epoxy-philic segment and an epoxy-phobic segment. The morphology adopted in the uncured state depends on the nature of the block polymer and the blend composition as incorporation of the thermosetting monomers into the epoxy-philic block compatible domains leads to predictable morphological transitions.[7] Typical bulk block polymer morphologies such as lamellar, gyroid, cylindrical and spherical,[5,7−9] and dilute solution morphologies, including spherical and wormlike micelles and vesicles,[10−13] have been observed. These morphologies can be frozen into the final structure upon curing often with minimal changes to the nanostructure.[7]

*To whom correspondence should be addressed. E-mail: hillmyer@umn.edu.

Seeking to expand the scope of block polymers to include systems where both blocks are miscible in the thermoset precursors, Meng et al. demonstrated that self-assembly of the block polymer prior to curing was not always necessary. To create a nanostructured thermoset using this approach, a block polymer with one segment that remained miscible in the thermoset throughout the cure and another block that phase separated upon curing was employed.[14] Phase separation during curing is induced by the decreasing entropic contributions to the free energy of mixing. Since the two blocks are covalently bound, phase separation is limited and nanostructured materials are formed. The final morphologies formed via this reaction-induced phase separation (RIPS) approach are microphase-separated, and the typical structures attained are trapped by gelation of the thermoset. Morphologies observed include dispersed and fused spherical particles, wormlike structures, bicontinuous structures, lamellae, and cylinders.[14−18]

Variations in the chemical composition,[14,17] number of blocks,[7,11] and architecture[9,18] of the block polymer additives have been explored. Additionally, reactive block polymers have been investigated as a means of fixing the morphologies and expanding the choice of precursors used in the thermoset.[19−28] The scope of thermosets investigated in these studies remains fairly narrow as epoxy thermosets[5,7,9−18,29−38] have received the bulk of the attention with only limited studies of phenolic[8,39,40] and unsaturated polyester resins.[41,42] Finally, applications of nanostructured thermosets using block polymers has primarily focused on their potential to improve the mechanical properties of the thermoset,[10,12,36,38] leaving a range of applications unexplored.

Our interest in the formation of nanostructured thermosets was motivated by the search for tough nanoporous membranes. We recently reported the formation of nanostructured poly(dicyclopentadiene) (PDCPD) by a RIPS process using a metathesis reactive block polymer: poly(norbornenylethylstyrene-*s*-styrene)-*b*-poly(lactide) (PNS−PLA).[43] In that example a tetrahydrofuran (THF) solution of PNS−PLA and DCPD was cross-linked using

 Published on Web 03/31/2010

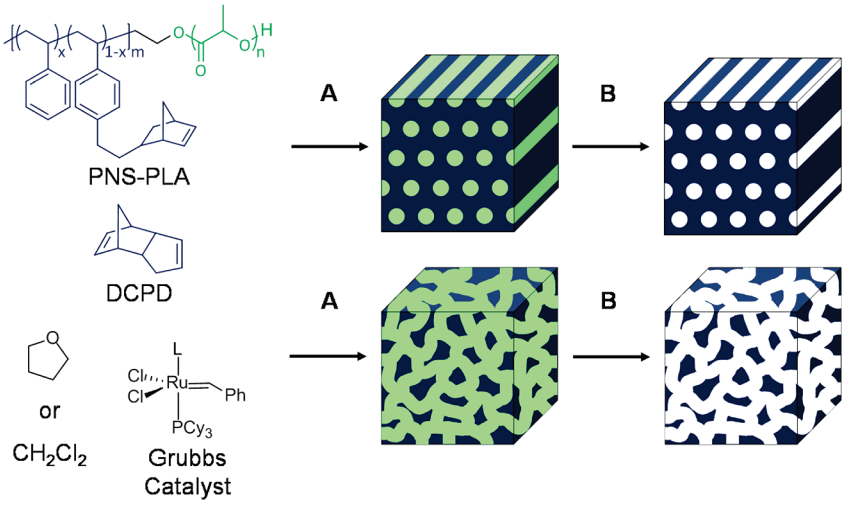

Figure 1. Pathways to nanoporous PDCPD via either self-assembly first (top) or RIPS (bottom). During step A of the self-assembly first approach the block polymer DCPD and the first generation Grubbs catalyst are dissolved in CH_2Cl_2, the CH_2Cl_2 is evaporated, the block polymer structure is aligned, and then the material is cross-linked. During step A of the RIPS approach a THF solution containing the block polymer and DCPD is cross-linked using the second generation Grubbs catalyst followed by evaporation of the solvent. During step B for both methods, the PLA component is removed by basic hydrolysis.

the second generation Grubbs catalyst (GII), and a nanostructured bicontinuous morphology resulted.[43] Alternatively, by incorporating the first generation Grubbs catalyst and evaporating the solvent, an ordered cylindrical morphology formed that could be fixed by cross-linking to create a nanostructured thermoset by a "self-assembly first" approach.[44] Both of these nanostructured thermosets were rendered nanoporous by selectively removing the PLA component. These two distinct approaches to nanoporous PDCPD are depicted schematically in Figure 1.

The reactive block polymer RIPS approach to nanostructured materials holds a great deal of promise for the formation of membranes with particularly attractive technological applications. We have demonstrated this in the area of the ultrafiltration of water,[45] the separation of N_2 and NH_3,[46] and polymer electrolyte membranes for direct methanol fuel cells.[47] Therefore, a detailed mechanistic understanding will enable the systematic tuning of the nanostructures and will be beneficial for the future development of these systems. Herein we provide insight into the mechanism of nanostructure formation in the RIPS protocol using DCPD and PNS−PLA. Our work includes how PLA block size and DCPD composition affected the final morphology of the material by a combination of small-angle X-ray scattering (SAXS), scanning electron microscopy (SEM), and nitrogen adsorption experiments.

Results

Synthesis and Characterization of PNS−PLA Block Polymers. PNS−PLA block polymers were previously synthesized by controlled radical polymerization using a PLA homopolymer functionalized with a chain transfer agent appropriate for controlled reversible addition−fragmentation transfer (RAFT) polymerization.[43,44] Various PLA block polymers[48−50] have also been prepared through the controlled ring-opening polymerization of lactide from a hydroxyl-terminated polymer.[51] We adopted this latter approach for the formation of PNS−PLA as shown in Figure 2.

Living anionic copolymerization of a mixture of styrene and norbornenylethylstyrene (N) followed by the addition of ethylene oxide produced a hydroxyl-functionalized PNS copolymer in 90% recovered yield. By ^{1}H NMR spectroscopy we determined that 14 mol % of N units was incorporated in

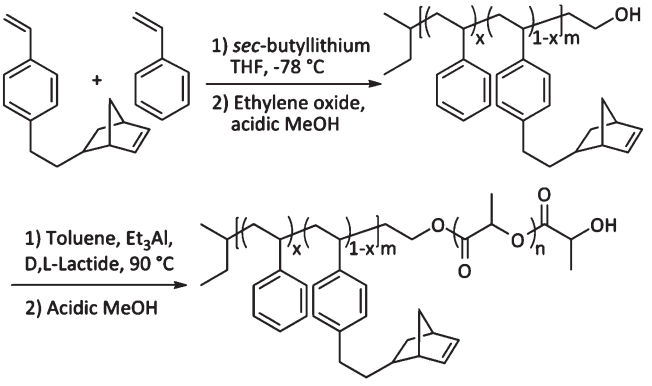

Figure 2. Synthetic scheme for the formation of PNS−PLA.

the PS block, and the number-average molecular weight (by end-group analysis) was 11 kg/mol. This number-average molecular weight was in good agreement with the value (11 kg/mol) determined by size exclusion chromatography using a light scattering detector. A polydispersity index (PDI) of 1.09 for this sample is consistent with the controlled nature of the polymerizations. The molecular weight and level of N incorporation compare favorably to the theoretical values of 10 kg/mol and 15 mol %, respectively. The slightly larger experimental molecular weight is attributed to potential contaminants in the N monomer that terminate some of the initiator or propagating chain ends. A comparison of the hydroxyl end groups to the *sec*-butyllithium end groups indicates 89% of the chains were successfully terminated with ethylene oxide. Although the copolymerization statistics were not investigated, it is expected that the norbornenylethyl substituent would be electron donating, which would decrease the stability of N-derived carbanion relative to styrene.[52] The difference in stability of styrene (M_1^-) relative to N (M_2^-) could lead to reactivity ratios of $r_1 > 1$ and $r_2 < 1$ similar to those observed for anionic polymerizations of styrene (M_1) and *p*-methylstyrene (M_2), $r_1 = 1.3$ and $r_2 = 0.9$,[53] or styrene (M_1) and *p*-*tert*-butylstyrene (M_2), $r_1 = 1.34$ and $r_2 = 0.86$.[54] In any case, the reactivity ratios for styrene and N are likely close to 1, and thus we expect a near random distribution of N units in the backbone.

Table 1. Molecular Characteristics of PNS−PLA Block Polymers

polymer	M_n (kg/mol)[a] PNS	x_N[b]	M_n (kg/mol)[a] PLA	PDI[c]	w_{PLA}[d]
PNS (11)	11	0.14		1.07	
PNS−PLA (11−15)	11	0.14	15	1.45	0.58
PNS−PLA (11−26)	11	0.14	26	1.54	0.70
PNS−PLA (11−42)	11	0.14	42	1.55	0.79
PNS−PLA (11−57)	11	0.14	57	1.34	0.84
PNS−PLA (15−30)	15	0.02	30	1.21	0.67

[a] Molecular weights were determined by ^{1}H NMR end-group analysis. [b] Mole fraction of N in the PNS block as determined by ^{1}H NMR spectroscopy. [c] PDI determined by size exclusion chromatography based on poly(styrene) standards. [d] Weight fraction of PLA ($w_{PLA} = M_{n,PLA}/(M_{n,PNS} + M_{n,PLA})$).

DL-Lactide was polymerized using triethylaluminum and the above hydroxy-terminated PNS to give a series of PNS−PLA block polymers. Molar masses of the PLA blocks were determined using ^{1}H NMR spectroscopy based on end-group analysis. SEC data exhibited a clear shift to lower elution volumes (see Figure S2) with increasing PLA molecular weight. A small amount of PNS homopolymer due to the incomplete end-capping with ethylene oxide (see above) was evident in the SEC data. All polymers are labeled PNS−PLA ($X-Y$) where X is the molar mass of the PNS block and Y is the molar mass of the PLA block in kg/mol. In addition to the PNS−PLA (11−Y) series, a PNS−PLA (15−30) sample with only 2 mol % N in the PNS block was prepared by the same protocol.

Nanoporous Thermoset Formation. Following the protocol we previously reported,[43] we prepared cross-linked films from solutions containing PNS−PLA and between 0 and 83 wt % DCPD (based on the total mass of PNS−PLA + DCPD). Briefly, a 75 wt % THF solution of the PNS−PLA and DCPD was combined with a 5 mg/mL THF solution of GII (0.5 wt % GII based on the total mass of the PNS−PLA and DCPD). In all cases, gelation occurred after ∼70 s.[55] After curing and drying overnight at room temperature, the samples were annealed at 100 °C for 1 h. The samples had contracted slightly due to the evaporation of the THF and densification. Based on their final mass after annealing, the samples contained 0−14 wt % THF. A list of the samples prepared using this general protocol is given in Table 2. All samples are labeled with the PNS−PLA sample code followed by DZ where Z is the DCPD wt % used to prepare the sample.

The samples were then subjected to basic hydrolysis to selectively etch the PLA block (see Experimental Section). The mass loss posthydrolysis was calculated as a percentage of the original mass of the cured sample (Table 2). The mass loss in the samples was generally comparable to the calculated PLA mass in the films based on the initial reactive mixture's composition. Some samples exhibited mass losses less than the initial amount of PLA, indicating that some PLA domains were inaccessible to the etching solution during the 72 h etch. In samples with mass losses greater than the initial PLA wt %, we suspect that the loss of any remaining THF or unreacted DCPD in the sample as well as small PDCPD fragments not effectively integrated into the sample was the cause. The biggest discrepancy was observed in samples containing 83 wt % DCPD.

Material Characterization. One-dimensional SAXS data acquired at room temperature for the PNS−PLA (11−15) and PNS−PLA (11−26) series of cross-linked films are given in Figure 3. Most of the samples exhibited a single broad peak characteristic of a nanophase-separated but disordered structure. After etching, the scattering intensity increased significantly for all samples consistent with formation of a nanoporous material (see Figure S4). The shape of most scattering profiles did not change upon etching consistent with preservation of the nanostructured morphology. The scattering profile for PNS−PLA (11−15) D83 before etching exhibited a broad scattering peak while after etching a scattering peak was not discernible likely due to the disruption of the nanostructure upon etching as the sample lost considerably more mass than the initial PLA wt %, leading to macropores near the bottom surface of the sample (see Figure S5). Scattering patterns of PNS−PLA (11−26) D83 and the PNS−PLA (11−42) and PNS−PLA (11−57) series (with the exception of the D0 samples before etching) did not exhibit a scattering maxima (see Figure S3) due to the lack of a nanophase-separated structure or because the domain spacing of the samples was greater than the range of the SAXS instrument (see below).

Table 2. Composition and Characterization Data for the Cross-Linked Films

film[a]	PLA (wt %)	mass loss[b] (wt %)	D (nm)[c] before etching	D (nm)[c] after etching	BET surface area (m^2/g)
PNS−PLA (11−15) D0	57	62	19	20	315
PNS−PLA (11−15) D17	48	54	21	21	265
PNS−PLA (11−15) D33	38	44	22	22	185
PNS−PLA (11−15) D50	29	8	23	23	3
PNS−PLA (11−15) D67	19	3	23	23	0
PNS−PLA (11−15) D83	10	21	25	*d*	0
PNS−PLA (11−26) D0	70	77	29	24	227
PNS−PLA (11−26) D17	58	66	29	28	253
PNS−PLA (11−26) D33	47	54	31	30	181
PNS−PLA (11−26) D50	35	41	36	36	94
PNS−PLA (11−26) D67	23	12	52	*d*	0
PNS−PLA (11−26) D83	12	29	*d*	*d*	0
PNS−PLA (11−42) D0	79	90	37	37	*e*
PNS−PLA (11−42) D17	66	74	*d*	*d*	167
PNS−PLA (11−42) D33	53	61	*d*	*d*	122
PNS−PLA (11−42) D50	40	49	*d*	*d*	76
PNS−PLA (11−42) D67	27	33	*d*	*d*	34
PNS−PLA (11−42) D83	13	54	*d*	*d*	3
PNS−PLA (11−57) D0	84	90	34	*d*	*e*
PNS−PLA (11−57) D17	70	76	*d*	*d*	131
PNS−PLA (11−57) D33	56	62	*d*	*d*	87
PNS−PLA (11−57) D50	42	48	*d*	*d*	67
PNS−PLA (11−57) D67	28	34	*d*	*d*	31
PNS−PLA (11−57) D83	14	25	*d*	*d*	7

[a] PNS−PLA (11−Y) DZ where Y is the molecular weight of PLA block in the block polymer (kg/mol) and Z is the DCPD wt % used to prepare the sample. All samples were prepared from a 75 wt % solution of THF and the components and were cross-linked with 0.5 wt % of GII. [b] Mass loss corresponds to the total percentage of mass loss upon etching the sample. [c] Domain spacings where determined from SAXS at room temperature using the Treubner−Strey microemulsion model. [d] A peak was not observed in the scattering pattern of these samples. [e] Surface area measurements were not performed on these samples as the samples were too mechanically weak to analyze.

We analyzed the scattering patterns that contained a well-defined SAXS peak using the Teubner−Strey microemulsion model (eq 1) given the bicontinuous structures observed by SEM (see below).[56]

$$I(q) \sim \frac{1}{a_2 + c_1 q^2 + c_2 q^4} \tag{1}$$

In eq 1, $I(q)$ is the intensity of the scattering, q is the principal scattering vector, and a_2, c_1, and c_2 are fitting constants.[57]

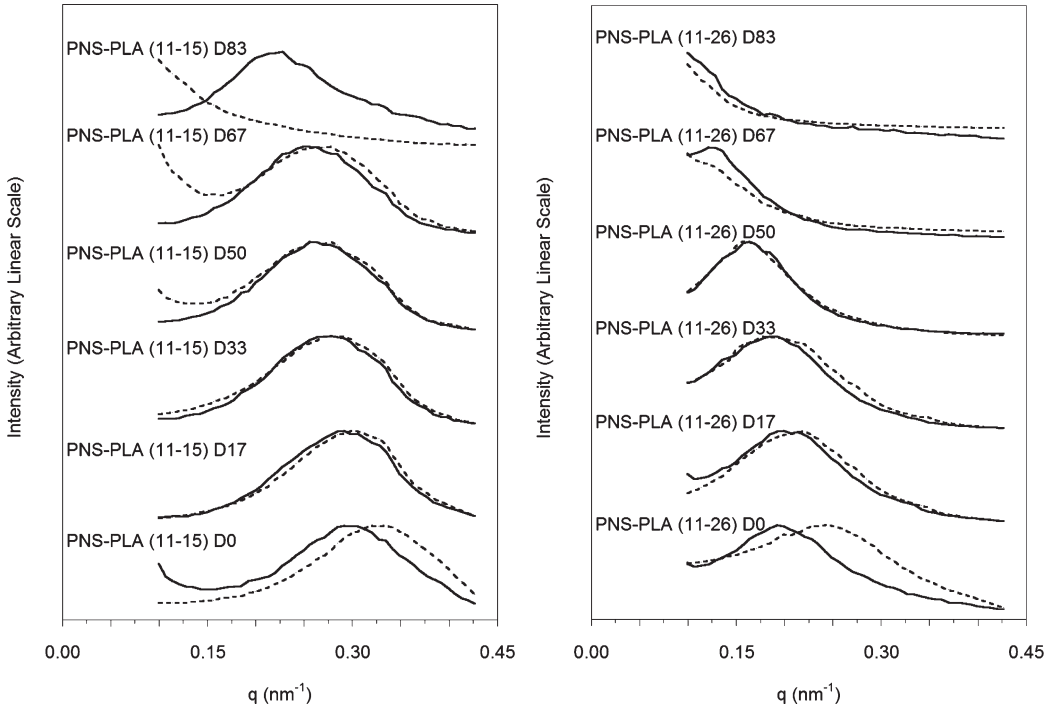

Figure 3. One-dimensional SAXS profiles for the PNS−PLA (11−15) (left) and PNS−PLA (11−26) (right) series of films acquired at room temperature. The solid and dashed lines are the scattering patterns before and after etching, respectively. Each set of scattering profiles was normalized to each other, and each set was shifted vertically for clarity.

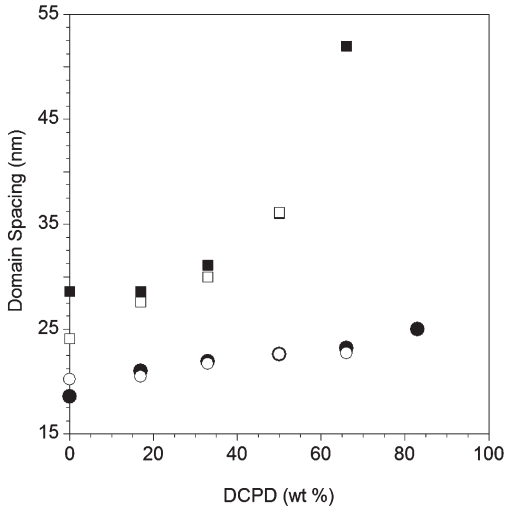

Figure 4. Domain spacing by SAXS analysis of the PNS−PLA (11−15) (circles) and PNS−PLA (11−26) (squares) series of films both before (filled) and after (open) etching as a function of DCPD wt %.

The principal domain spacing (D) can be extracted from the fitting constants using eq 2.[57]

$$D = 2\pi\left[\frac{1}{2}\left(\frac{a_2}{c_2}\right)^{1/2} - \frac{1}{4}\frac{c_1}{c_2}\right]^{-1/2} \quad (2)$$

In the PNS−PLA (11−15) and PNS−PLA (11−26) samples, D increased with increasing fraction of DCPD in the samples (Figure 4). This is consistent with trends observed in other nanostructured thermosets formed via RIPS.[14,15,17]

SEM micrographs of cryo-fractured surfaces of the samples coated with 1.5 nm of platinum (Figure 5) revealed that most of the etched films have a nanoporous bicontinuous morphology including the PNS−PLA (11−42) and PNS−PLA (11−57) containing samples that did not exhibit a peak in the SAXS data. Domain spacings for these samples based on the SEM micrographs were >65 nm, and such large domain spacings would be difficult to discern given the range of the SAXS instrument. The micrographs also reveal that increasing PLA block size at fixed DCPD composition leads to increasing pore size (consistent with the SAXS data), while increasing the DCPD composition at fixed PLA block size leads to a coarsening of the structure. Additionally, unlike the other samples, the PNS−PLA (11−15) D50, PNS−PLA (11−15) D67, and PNS−PLA (11−26) D67 samples exhibited largely nonporous morphologies, which is consistent with the inability to etch all of the PLA based on the mass loss data (Table 2).

The morphology of the PNS−PLA (11−Y) D83 films could not be adequately characterized by a single micrograph. Figure 6 shows an example cross section of the PNS−PLA (11−26) D83 sample. Region A is close to the surface of the film exposed to air and was essentially nonporous. Region B in the middle of the film contains both porous and nonporous areas. Region C depicts the section of the film in contact with the glass vial used to prepare the sample. This section of the film is quite similar to the bicontinuous morphology observed for the other samples except it has larger pores and a broader pore size distribution. These data indicate that in samples with a large DCPD content the formation of composite materials is more complicated than in the samples with less DCPD.

Nitrogen adsorption analysis of the etched samples resulted in isotherms similar to type IV isotherms typical of mesoporous materials (see Figure S8).[58] Surface areas were calculated using the Brunauer−Emmett−Teller (BET) multipoint method[59] (Table 2). Pore size distributions were determined using the Barrett−Joyner−Halenda (BJH) approach[60] and are shown for the D33 samples and the PNS−PLA (11−15) containing series in Figure 7.

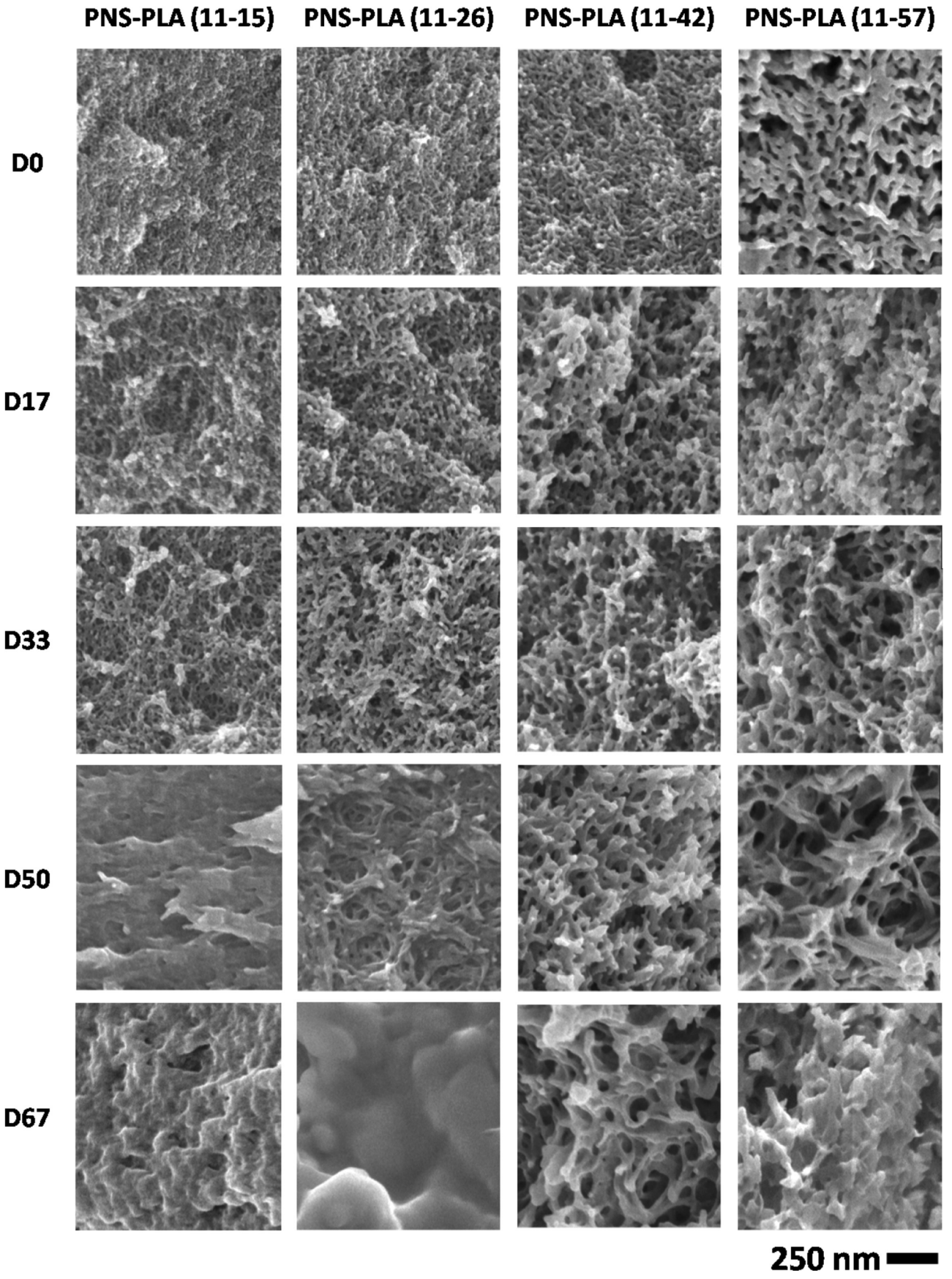

Figure 5. Scanning electron micrographs of fractured surfaces of etched films. All samples were cryo-fractured and coated with 1.5 nm of platinum prior to imaging to prevent charging.

The D33 series of films shows that as the PLA block size increases the pore size distribution shifts to larger diameters, which corroborates trends in both the SAXS and SEM data. Additionally, the BET surface areas decrease from 185 to 87 m^2/g (Table 2) upon increasing the PLA molar masses from 15 to 57 kg/mol. Pore sizes for the PNS−PLA (11−15) samples are essentially constant with increasing weight percent of DCPD (up to 33 wt % DCPD). While the single PLA block size led to relatively consistent pore sizes, the BET surface area of these films decreases with increasing DCPD concentration from 315 to 185 m^2/g for DCPD concentrations ranging from 0 to 33 wt %. Given the consistent pore size distribution in these samples, the surface area of the films decreases linearly with decreases in the volume fraction of PLA in the composite as expected for a fixed pore size. At higher DCPD compositions, the PNS−PLA (11−15) samples had very little or immeasurable surface areas consistent with the SEM micrographs of the D50 and D67 samples.

The trend of a decreasing surface area observed for the PNS−PLA (11−15) samples was also observed for the other block polymer samples at higher DCPD compositions. A surface area was determined for the PNS−PLA (11−26) D50 sample; however, samples areas for the D67 and D83 samples were not measurable. Surface areas for the PNS−PLA (11−42) and PNS−PLA (11−57) samples decreased linearly with decreases in PLA volume fraction at all DCPD compositions.

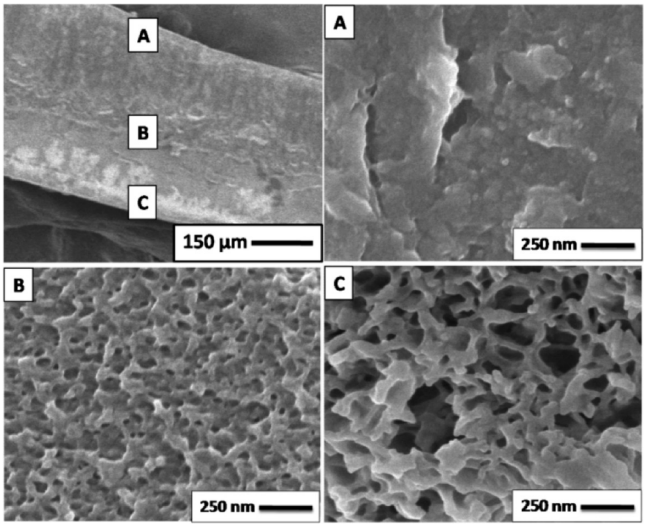

Figure 6. Scanning electron micrographs of a fractured surface of the PNS−PLA (11−26) D83 film. Cross section of the entire film (top left), with the three regions highlighted corresponding to the other three micrographs (A, B, and C) shown.

Discussion

We demonstrated that the metathesis cross-linking of a THF solution of DCPD in the presence of a PNS−PLA block polymer can yield a nanostructured PDCPD/block polymer composite sample, and the PLA in these samples can be etched to generate nanoporous materials. Pore sizes could be tailored by adjusting the size of the PLA block, and the porosity was controlled by varying the DCPD content in the composites. We leave the balance of the paper to discuss the mechanism of structure formation in these composites. That is, how does a homogeneous solution containing DCPD, PNS−PLA, and THF give the observed structures upon addition of a metathesis catalyst?

Mechanism Investigation. In our initial attempts to form nanostructured PDCPD composites we employed a nonreactive PS−PLA block polymer and a potentially reactive (i.e., double bond containing) poly(butadiene) [PB]−PLA block polymer using a similar protocol to that described above. In all cases, brittle opaque materials were formed consistent with macrophase separation. We hypothesized that the reactive block needed to be capable of fully and rapidly cross-linking into matrix to prevent macrophase separation, and thus we subsequently developed the metathesis reactive monomer N for incorporation into PS−PLA block polymers. Inclusion of the reactive component led to the successful formation of PDCPD with a bicontinuous nanostructure; this strategy prevented macrophase separation.[43]

To probe the number of cross-linkable groups necessary for achieving a nanostructured sample, a PNS−PLA (15−30) block polymer was prepared with 2 mol % N per chain. Cross-linked DCPD films with PNS−PLA (15−30) led to the formation of nanophase-separated structures based on SAXS analysis, and SEM images of an etched sample revealed a nanoporous bicontinuous structure (see Figure S10). The success of a block polymer with so few cross-linkable units led us to synthesize a metathesis reactive end-functionalized PLA homopolymer by the ROP of lactide initiated by 2-hydroxymethyl-5-norbornene. Use of this end-functionalized PLA in our standard RIPS process with DCPD resulted in macrophase separation. These results revealed that while minimal reactive norbornenes per PLA chain are needed for effective nanostructure formation, inclusion of them in a block polymer appears to be necessary; norbornene end-functionalized PLA is apparently not sufficient.

The structures formed using the above approach are kinetically trapped, and thus we examined the influence of

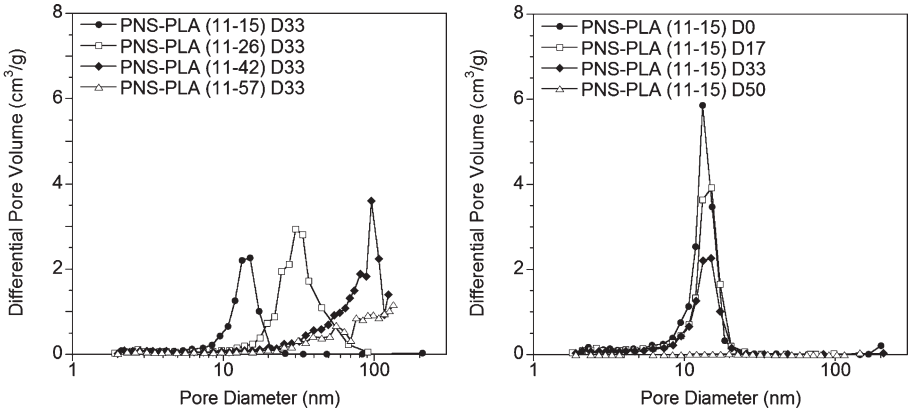

Figure 7. BJH pore size distributions for the D33 series of films (left) and PNS−PLA (11−15) series of films (right). The differential pore volume is defined as the d(incremental pore volume)/d(log pore diameter).

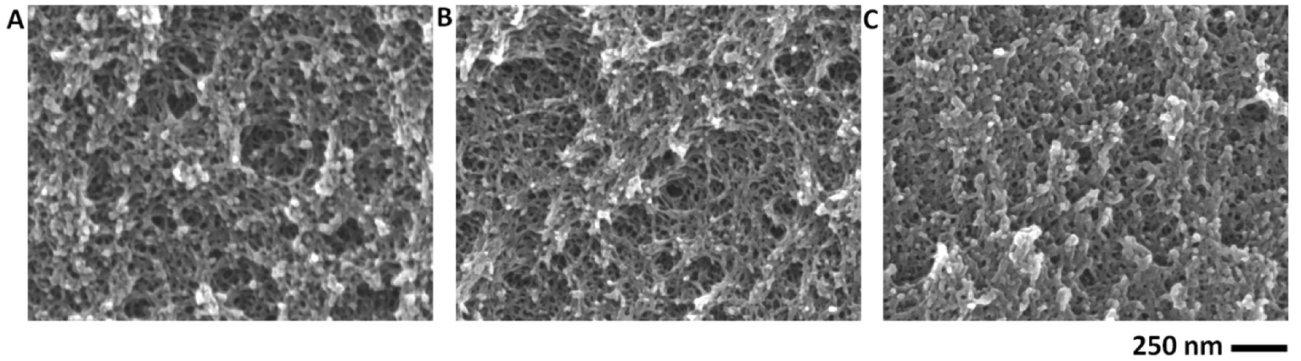

Figure 8. Scanning electron micrographs of fractured surfaces of etched PNS−PLA (11−15) D33 films cross-linked with (A) 5, (B) 0.5, and (C) 0.05 wt % of GII.

gelation time on the final structure in a series of PNS−PLA (11−15) D33 films cross-linked with 5, 0.5, and 0.05 wt % GII. The films gelled almost instantly (5%), at 70 s (0.5%), and at 13 min (0.05%). SAXS patterns (see Figure S11) exhibited a single broad scattering peak for all three samples with average domain spacings of 23, 21, and 21 nm for the 5%, 0.5%, and 0.05% films, respectively. SEM images of etched films revealed bicontinuous structures (Figure 8) in all cases. The small changes in domain spacing and lack of variation among the SEM micrographs suggest that the timing of gelation does not significantly impact resultant structures. Thus, coarsening of the structure during the RIPS process does not seem to be occurring to a significant extent. An alternative conclusion is that the structure forms via a self-assembly first mechanism. However, as previously reported in ref 32, dynamic light scattering (DLS) analysis of a THF solution of PNS−PLA and DCPD prior to catalyst addition did not indicate any aggregation of the block copolymer chains (i.e., micelle formation), suggesting that the chains were simply dissolved in the solvent mixture prior to cross-linking. From a practical view, using less catalyst to obtain the same structure is desirable. Although the impact of the mechanical properties was not investigated, a decrease in the catalyst concentration could lead to a decrease in the cross-linking density, possibly leading to weaker materials.

To track the structure development upon cross-linking, we explored the evolution of the SAXS data as a function of cross-linking time. In our initial SAXS experiments we monitored structure development well into the cross-linking and observed a shift of the principal scattering peak to lower values of q (larger domain spacings). At longer cross-linking times, electron density contrast was lost, and no further information could be gathered. To overcome this limitation, a PNS−PLA (11−15) D33 solution was prepared in benzene and divided among five ampules. To four ampules 0.25 wt % of GII was added, and the samples were cross-linked for 10 s, 1 min, 8 min, and 1 h. After the designated times, further structure development was arrested by immersion in a liquid nitrogen bath, and the benzene was removed by sublimation (i.e., freeze-dried). In this way, we can interrogate the partially cured samples to get a sense of how and when the nanostructure is formed. In addition to the freeze-dried samples, the mixture in the fifth ampule was cross-linked by our normal solvent evaporation protocol over (24 h) using 0.25 wt % GII. SAXS patterns for all the dried samples are shown in Figure 9.

The SAXS patterns show the emergence of a scattering peak at 10 s, which first shifts to low q and then back to high q. These general shifts in the scattering profile qualitatively match changes observed during our original in situ SAXS

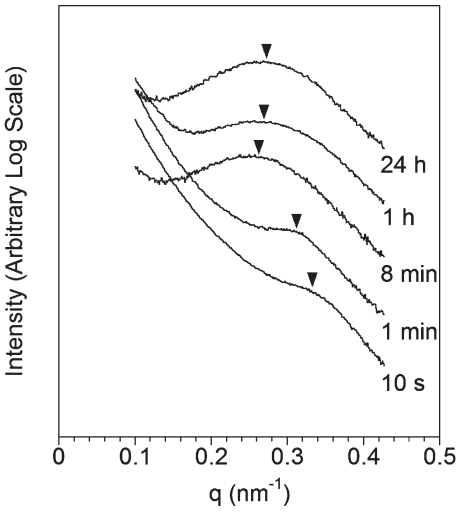

Figure 9. One-dimensional SAXS profiles for PNS−PLA (11−15) D33 samples freeze-dried after 10 s, 1 min, 8 min, and 1 h of cross-linking. The 24 h sample was not freeze-dried as the solvent had already evaporated. The arrow denotes the peak maximum.

experiments. The initial peak observed at 10 s corresponds to a domain spacing of 19 nm and indicates that the sample is already phase separated due to the increasing molecular weight of the cross-linking components. At 1 and 8 min the domain spacings were 20 and 24 nm, respectively. The domain spacing increased as the material further organized until gelation was reached at about 90 s. Upon gelation, the material is a swollen network, and the domain spacing decreases to 23 nm as swelling within the material reduces due to concomitant evaporation of solvent. Finally, after 24 h all the solvent has evaporated, and the scattering vector shifts to slightly higher values, resulting in a domain spacing of 22 nm.

The change in domain spacing upon solvent evaporation was corroborated by first swelling a cross-linked and dried PNS−PLA (11−26) D50 sample in THF. The swollen sample was then analyzed by SAXS every 10 min over a 40 min span while the THF evaporated. At the beginning of the drying experiment, the sample did not have an observable scattering peak likely due to a lack of electron density contrast, but a broad peak was observed after 10 min of drying at RT that shifted to higher q values at longer times. The unswollen sample originally had a domain spacing of 34 nm, which after swelling shifted to 39 nm at 10 min, 38 nm at 20 min, 37 nm at 30 min, and 36 nm at 40 min. Qualitatively, the shift in domain spacing observed for the cross-linked swollen sample is in good agreement with the decrease

in domain spacing after gelation in the freeze-dried samples, supporting the conclusion that the change in domain spacings are due to evaporation of the solvent.

Morphological Control. The SEM micrographs in Figure 7 revealed that most samples exhibited bicontinuous nanoporous morphologies while a few were nonporous. Specifically, films PNS−PLA (11−15) D50, PNS−PLA (11−15) D67, and PNS−PLA (11−26) D67 were largely nonporous, indicating possible encapsulation of PLA within the matrix, which was corroborated by the mass loss data for those samples (Table 2). These samples illustrate that there is an upper limit to the level of DCPD incorporation in PNS−PLA (11−15) and PNS−PLA (11−26) samples required to access a bicontinuous structure. On the other hand, films templated with PNS−PLA block polymers containing larger PLA blocks retained bicontinuous structures at higher DCPD fractions. For example, in the case of the PNS−PLA (11−42) and PNS−PLA (11−57) templated membranes, bicontinuous structures were observed using up to 67 wt % DCPD.

We examined the effect of PLA block length (composition) on the nature of the reactive solution prior to cross-linking. Previous DLS results suggested that prior to cross-linking the PNS−PLA chains were simply dissolved in the mixture of THF and DCPD.[43] To complement that study, we examined the extent of overlap of the PNS−PLA block polymers in solution as this could influence the final morphology. The overlap concentration (c^*) for the polymer chains can be estimated by eq 3.[61]

$$c^* = \frac{3M}{N_{av} 4\pi {R_g}^3} \tag{3}$$

where M is the molecular weight of the block polymer, N_{av} is Avogadro's number, and R_g is the radius of gyration. The radius of gyration was estimated based on the hydrodynamic radius (R_h) measured for the free chains in THF using DLS (see Supporting Information) and the relationship in eq 4.[62]

$$R_g = \frac{R_h}{0.66} \tag{4}$$

Table 3 contains the calculated c^* for the block polymers in mg/mL and an extent of overlap c/c^* for each sample. The transition between nonbicontinuous and bicontinuous structures was within c/c^* ranges of 1.8−2.5 for PNS−PLA (11−15), 1.5−2.2 for PNS−PLA (11−26), 1.0−2.0 for PNS−PLA (11−42), and 1.1−2.3 for PNS−PLA (11−57) solutions. From these data, it appears that the critical concentration (i.e., extent of overlap) to achieve a bicontinuous structure is around $2c^*$.

Table 3. Estimated Overlap Concentration (c^*) for the PNS−PLA Block Polymers and the Ratio of c/c^* for Each of the DCPD Solutions Prior to Cross-Linking[a]

	PNS−PLA (11−15)	PNS−PLA (11−26)	PNS−PLA (11−42)	PNS−PLA (11−57)
c^* [b]	82	68	51	44
c/c^* D0	*3.7*	*4.4*	*5.9*	*6.8*
c/c^* D17	*3.1*	*3.7*	*4.9*	*5.7*
c/c^* D33	*2.5*	*2.9*	*3.9*	*4.5*
c/c^* D50	**1.8**	*2.2*	*3.0*	*3.4*
c/c^* D67	**1.2**	**1.5**	*2.0*	*2.3*
c/c^* D83	**0.6**	**0.7**	**1.0**	**1.1**

[a] Final cross-linked samples that were determined to be bicontinuous are in italics, and samples that were nonbicontinuous are in bold. [b] Calculated overlap concentration for the block polymer in mg/mL based on DLS results (see Supporting Information).

The apparent relation between the morphology and the extent of block polymer overlap sheds light on the structure formation mechanism. Initially, the cross-linking solution contains solvent (i.e., THF), DCPD, and PNS−PLA. After adding the catalyst, the PNS block and DCPD cross-link, and their increasing molecular weight increases the free energy of mixing with the PLA until the PLA block phase separates from the developing PNS/PDCPD matrix. If the block polymer was well overlapped, a bicontinuous structure forms to best minimize interfacial tension with the matrix material. That is, isolated domains of PLA would have a higher interfacial area with the PNS/PDCPD matrix than a percolating 3-D structure at the same volume fraction.[63] At lower block polymer concentrations the PLA chains are more easily encapsulated and form isolated domains in the developing PNS/PDCPD matrix.

To examine the morphological dependence on the extent of overlap, two PNS−PLA (11−26) D33 samples were cross-linked at 85 and 92 wt % THF instead of the 75 wt % used in all of the above experiments. Dilution of the cross-linking solution caused a delay in gelation from 70 s at 75 wt % to 3 min at 85 wt % while the 92 wt % sample did not form a gel but ultimately solidified as a coating on the sample vial after 16 h. SEM micrographs of freeze-fractured surfaces of etched films are shown in Figure 10. The 85 wt % sample appears to have a bicontinuous structure, but the structure is more open than the 75 wt % sample. The 92 wt % sample has some bicontinuous areas, but the structure is more collapsed and less uniform than the other two samples.

The c/c^* ratio was 2.9, 1.5, and 0.7 for the 75, 85, and 92 wt % samples, respectively. The formation of a bicontinuous structure at a c/c^* of 1.5 for the 85 wt % sample is just at the edge of the transition range for the PNS−PLA (11−26) samples (1.5−2.2) as determined above. The c/c^* ratio for the 92 wt % sample was 0.7, which is below the range of the bicontinuous structures observed for the PNS−PLA

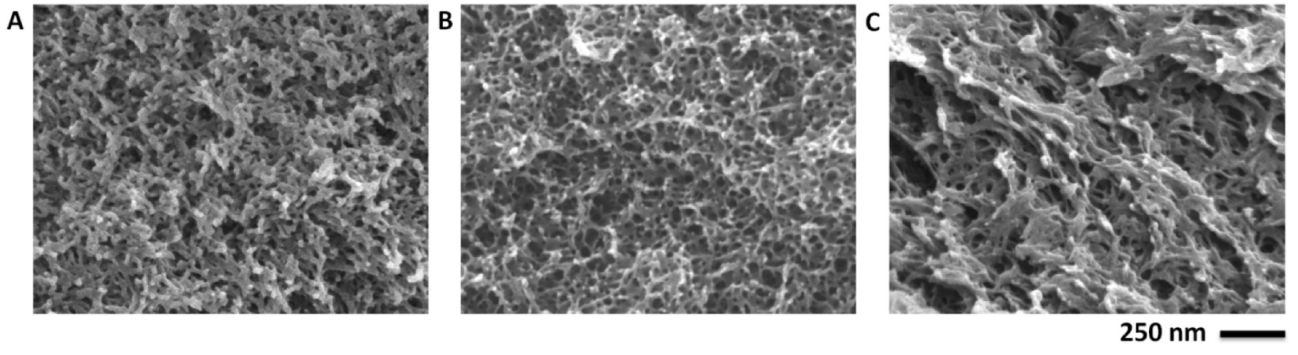

Figure 10. Scanning electron micrographs of fractured surfaces of PNS−PLA (11−26) D33 samples cast at (A) 75, (B) 85, and (C) 92 wt % THF.

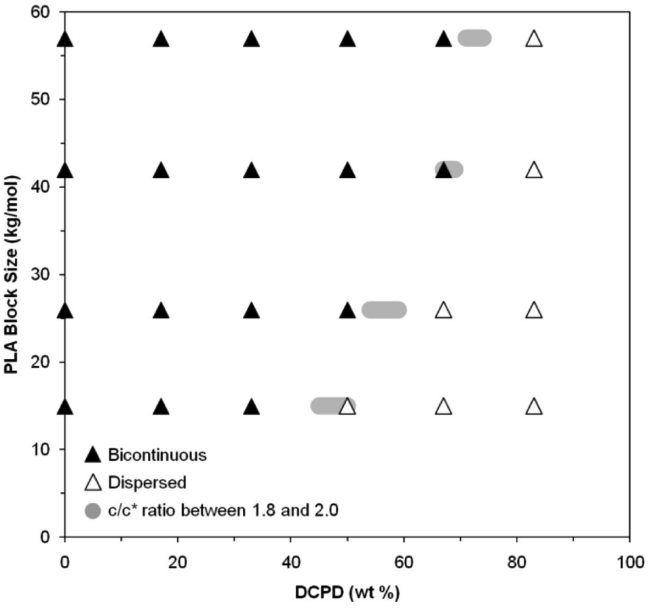

Figure 11. Phase diagram of the films formed in this study where the filled triangles represent bicontinuous structures and the empty triangles represent structures with isolated PLA domains (i.e., nonbicontinuous). The gray areas depict compositions with c/c^* ratios between 1.8 and 2.0 for the block polymers assuming a THF composition of 75 wt %.

(11−26) samples, and the formation of a more collapsed structure with nonbicontinuous areas is consistent with the morphological dependence on the extent of overlap.

The above analysis allows for structure predictions based on the block polymer molecular weight and composition of the solution prior to cross-linking. Figure 11 shows a morphology map for the films formed in this study. It also illustrates compositions of the smaller overlapping c/c^* range (1.8−2.0) for the four block polymers at a THF composition of 75 wt % (gray areas). Compositions to the upper left of these regions would be more overlapped and likely result in a bicontinuous morphology, while compositions to the lower right would be less overlapped and likely result in encapsulated PLA domains and nonbicontinuous samples.

Summary

We explored the templating of nanostructures within a DCPD thermoset by a metathesis reactive block polymer, PNS−PLA. Nanophase-separated morphologies from homogeneous solutions of the components formed via a RIPS mechanism. Mechanistic investigations revealed that cross-linking the PNS block into the thermoset matrix was vital to limiting macrophase separation and that the morphologies were unaffected by altering the catalyst concentration. Examining a wide range of compositions with multiple PLA block lengths revealed that the pore size and surface area of the materials can be tailored by changing the PLA block size and DCPD composition, respectively. Additionally, a transition from a bicontinuous morphology to an encapsulated morphology was observed in the samples. The morphology formed was found to depend on the concentration of block polymer relative to the overlap concentration, allowing for morphological control and predictions based on the block polymer size and cross-linking solution composition.

Experimental Section

Materials. Unless specifically noted, all chemicals were used as received from Aldrich. Styrene was first passed through a basic alumina column and then distilled over calcium hydride under reduced pressure. Ethylene oxide was distilled over butylmagnesium chloride under reduced pressure. 4-Chloromethylstyrene was passed through a basic alumina column. DL-Lactide (99%) purchased from Purac was recrystallized twice from ethyl acetate and stored under a N_2 atmosphere. GII was a gift from Materia and was used as received. Degassed THF was purified by passage over an activated alumina column, while degassed toluene was purified by passage over an activated alumina column and supported copper catalyst column to remove protic impurities and oxygen prior to use.

Characterization. ^{1}H NMR spectroscopy was performed on a Varian Inova 500 instrument operating at 500 MHz. Solutions were prepared in $CDCl_3$ (Cambridge Isotope Laboratories) at ~10 mg/mL. All spectra were obtained at 20 °C after 64 transients using a relaxation delay of 5 s with chemical shifts reported as δ (ppm) relative to the ^{1}H signals from hydrogenous solvent (7.27 ppm for $CHCl_3$).

SEC was used to evaluate the molecular weight evolution and polydispersity indicies of all the samples. Samples were prepared at concentrations near 1 mg/mL in $CHCl_3$ or THF depending on the instrument used. The first SEC instrument operates at 35 °C with $CHCl_3$ as the mobile phase through three PLgel 5 μm Mixed-C columns in series with molecular weight range 400−400 000 g mol^{-1}. The columns are housed in a Hewlett-Packard (Agilent Technologies) 1100 series liquid chromatograph equipped with a Hewlett-Packard 1047A refractive index detector. PDIs are reported with respect to polystyrene standards obtained from Polymer Laboratories. A second SEC instrument is a Waters 150 CALC/GPC instrument using three Phenomenex Phenogel columns of 103, 104, and 105 Å porosities coupled with a Wyatt OPTILAB refractive index detector and a Wyatt DAWN multiangle light-scattering detector. This instrument operates at 40 °C with THF as the mobile phase and a flow rate of 1 mL/min.

SAXS profiles were recorded on a custom-built beamline at the University of Minnesota. Cu Kα X-rays (λ = 1.542 Å) were generated through a Rigaku RU-200BVH rotating anode fitted with a 0.2 × 2 mm^2 microfocus cathode and Franks mirror optics. Two-dimensional (2-D) diffraction patters were recorded for 300 s using a Siemens area detector and corrected for detector response before analysis. 2-D images were azimuthally integrated to a 1-D plot of intensity versus q.

SEM images were obtained on a Hitachi S-900 FE-SEM instrument using a 3.0 kV accelerating voltage. Prior to SEM analysis, cryo-fractured monoliths were coated with a 1.5 nm thick platinum layer via direct platinum sputtering using a VCR ion beam sputter coater. Nitrogen adsorption experiments were carried out on a Micromeritics ASAP 2000 V3.00 sorption analyzer, and samples were prepared by degassing under high vacuum at 60 °C for at least 6 h.

Samples were prepared for DLS by dissolving each block polymer at 2 wt % in THF. The block polymer solutions were then filtered through 0.45 μm microfilters (Millipore) into dust-free 0.25 in. diameter glass tubes. Samples were immersed in a temperature-controlled silicon oil bath inside a home-built goniometer, and DLS measurements were performed using a Lexel model 75 Ar^+ ion laser with a 488 nm operating wavelength. A Brookhaven BI-DS photomultiplier was used to detect the scattered light intensity, and the resulting signal was processed using a BI-9000AT digital correlator. The intensity autocorrelation function was measured over an hour for each polymer at 25 °C and angles of 60°, 90°, and 120°, and the resulting data were processed as outlined in the Supporting Information.

Synthesis. *Synthesis of Hydroxyl-Terminated Poly(norbornenylethylstyrene-s-styrene) (PNS-OH).* PNS-OH was prepared in an approach adapted from a previously reported method for the synthesis of hydroxyl-terminated polystyrene.[50] A 1 L round-bottom flask adapted with five threaded glass connectors was heated at 250 °C overnight under vacuum. Then a glass stir

bar and *p*-norbornenylethylstyrene (2.02 g, 9.02 mmol), prepared via previously reported methods,[43,44] were added under a positive pressure of argon. Next a buret of purified styrene (4.79 g, 46.1 mmol), a buret of purified ethylene oxide (5.40 g, 123 mmol), and a flask of 0.3 L of purified THF were connected to the reaction flask via threaded glass connectors. Five pump purge cycles with argon were performed on the reaction flask before it was pressurized with argon. THF was added to the reaction flask, which was submerged in an isopropyl alcohol/dry ice bath. The styrene was then added to the reaction flask, followed by the addition of *sec*-butyllithium (0.70 mL, 0.49 mmol). The polymerization was allowed to proceed for 30 min, and then the ethylene oxide was added. The solution was slowly warmed to room temperature over an hour and allowed to stir overnight. The alkoxy chain end was terminated by the addition of 3 mL of a 1 M hydrochloric acid solution in methanol that had been degassed by bubbling with argon for 15 min and allowed to stir for 1 h before being precipitated methanol. The precipitate was recovered by vacuum filtration and then reprecipitated in methanol from THF. The precipitate was again recovered via vacuum filtration before being dried under vacuum for 48 h. 6.193 g of a white powder was recovered for a yield of 90.1%. Number-average molecular weight of the polymer was 11 kg/mol with a 14% mole fraction of norbornenylethylstyrene as determined by ^{1}H NMR end-group analysis. SEC analysis determined a PDI of 1.09. ^{1}H NMR ($CDCl_3$): δ 6.30−7.20 (b, Ar**H**), 5.90−6.20 (b, −C**H**=C**H**−), 3.27 (b, −C**H**$_2$−OH), 2.78−2.81 (−C**H**−CH$_2$=CH$_2$−C**H**−), 2.53 (b, Ar−C**H**$_2$−), 2.02 (b, −C**H**−CH$_2$−CH$_2$−Ar), 1.86 (b, −CH−C**H**$_2$**(exo)** −CH−), 1.41 (b, −CH−C**H**$_2$−CH− and −C**H**$_2$−CH$_2$−Ar), 1.23 (b, −CH−C**H**$_2$−CH), 0.9 (b, −C**H**$_2$− of initiator), 0.7 (b, −C**H**$_3$ of initiator), 0.56 (b, CH−CH$_2$-**(endo)**=CH).

Synthesis of Poly(norbornenylethylstyrene-s-styrene)-b-Poly(lactide) (PNS−PLA). All PNS−PLA block copolymers were synthesized following the same general procedure based on the ROP of lactide using a triethylaluminum PNS-OH macroinitiator. An example synthesis is described for PNS−PLA (11−15). 2.00 g (0.154 mmol) of PNS (11) and a Teflon stir bar were added to a 48 mL round-bottom pressure vessel capped with a Teflon screw-cap. The pressure vessel was placed in a glovebox under a nitrogen atmosphere, and 25 mL of toluene and 75 μL (0.75 mmol) of a 1 M triethylaluminum solution in heptanes were added via a graduated cylinder and a syringe, respectively. The pressure vessel was capped and stirred for 16 h, and then 3.331 g (23.1 mmol) of DL-lactide was added. The pressure vessel was capped and removed from the glovebox and heated at 105 °C for 5 h. The polymerization was terminated by the addition of 2 mL of a 2 M hydrochloric acid solution in methanol, and the polymerization solution was then precipitated in methanol. The precipitate was recovered via vacuum filtration and reprecipitated in methanol from THF. The precipitate was once again recovered via vacuum filtration and dried under vacuum for 48 h. 4.740 g of a white solid was recovered for a yield of 89.0%. Number-average molecular weight of the polymer was 15 kg/mol as determined by ^{1}H NMR end-group analysis, while the PDI was 1.45 as determined by SEC. ^{1}H NMR ($CDCl_3$): δ 6.30−7.20 (b, Ar**H**), 5.90−6.20 (b, −C**H**=C**H**−), 5.13−5.24 (m, −C(O)−C**H**(CH$_3$)−O−), 4.36 (m, −C(O)−C**H**(CH$_3$)−O− end group), 2.78−2.81 (−C**H**−CH$_2$=CH$_2$−C**H**−), 2.53 (b, Ar−C**H**$_2$−), 2.02 (b, −C**H**−CH$_2$−CH$_2$−Ar), 1.86 (b, −CH−C**H**$_2$**(exo)** −CH−), 1.57 (b, −C(O)−CH(C**H**$_3$)−O−), 1.41 (b, −CH−C**H**$_2$−CH− and −C**H**$_2$−CH$_2$−Ar), 1.23 (b, −CH−C**H**$_2$−CH), 0.9 (b, −C**H**$_2$− of initiator), 0.7 (b, −C**H**$_3$ of initiator), 0.56 (b, CH−CH$_2$(**endo**)=CH).

Preparation of Nanoporous Films. Films were formed by dissolving the PNS−PLA template and DCPD in 1.0 mL of THF at the desired compositions followed by the addition of a GII in solution (0.2 mL). After stirring for 10 s, the stir bar was removed; the vial was placed under a crystallization dish, and the solution was allowed to cross-link for 18 h. The film was then uncovered and placed in an oven at 100 °C to anneal the film. Films were then cut into smaller pieces (approximately 5 mm × 3 mm × 1 mm), immersed in a 0.5 M NaOH solution (40/60 by volume of methanol and water), and heated at 70 °C for 3 days to remove the PLA. Resultant monoliths were washed with methanol and dried under vacuum for 24 h.

Acknowledgment. This work was largely supported by the U.S. Department of Energy (Grant No. 5-35908). We also acknowledge the Abu Dhabi-Minnesota Institute for Research Excellence (ADMIRE); a partnership between the Petroleum Institute (PI) of Abu Dhabi and the Department of Chemical Engineering and Materials Science of the University of Minnesota. M.A.A. acknowledges financial support from the U.S. Air Force. Parts of this work were carried out in the University of Minnesota I.T. Characterization Facility, which receives partial support from NSF through the NNIN program. The authors thank Chun Liu for assistance with the DLS measurements and Professor Tim Lodge for helpful discussions about the DLS data. The authors also thank Louis Pitet for helpful input.

Supporting Information Available: ^{1}H NMR spectra of PNS homopolymer and PNS−PLA block polymer, SEC chromatograms of PNS homopolymer and PNS−PLA (11−*Y*) block polymers, SAXS profile of PNS−PLA (11−42) and PNS−PLA (11−57) series of films, Teubner−Strey microemulsion fit of PNS−PLA (11−15) D17 sample, SEM micrographs of PNS−PLA (11−*Y*) D83 samples, nitrogen adsorption/desorption isotherms, BJH pore size distributions for the PNS−PLA (11−26), PNS−PLA (11−42), and PNS−PLA (11−57) samples, SEM micrographs of PNS−PLA (15−30) D33 and norbornene-functionalized PLA homopolymer (40%) with DCPD (60%) samples, SAXS profile of PNS−PLA (11−15) D33 samples cross-linked with 5%, 0.5%, and 0.05% catalyst, and DLS analysis of the block polymer chains. This material is available free of charge via the Internet at http://pubs.acs.org.

References and Notes

(1) Zammarano, M.; Franceschi, M.; Bellayer, S.; Gilman, J. W.; Meriani, S. *Polymer* **2005**, *46*, 9314–9328.
(2) Nelson, J. K.; Hu, Y. *J. Phys. D* **2005**, *38*, 213–222.
(3) Douglas, E. P. *Polym. Rev.* **2006**, *46*, 127–141.
(4) Jeong, W.; Kessler, M. R. *Chem. Mater.* **2008**, *20*, 7060–7068.
(5) Hillmyer, M. A.; Lipic, P. M.; Hajduk, D. A.; Almdal, K.; Bates, F. S. *J. Am. Chem. Soc.* **1997**, *119*, 2749–2750.
(6) Bates, F. S.; Fredrickson, G. H. *Annu. Rev. Phys. Chem.* **1990**, *41*, 525–557.
(7) Lipic, P. M.; Bates, F. S.; Hillmyer, M. A. *J. Am. Chem. Soc.* **1998**, *120*, 8963–8970.
(8) Kosonen, H.; Ruokolainen, J.; Nyholm, P.; Ikkala, O. *Macromolecules* **2001**, *34*, 3046–3049.
(9) Serrano, E.; Tercjak, A.; Kortaberria, G.; Pomposo, J. A.; Mecerreyes, D.; Zafeiropoulos, N. E.; Stamm, M.; Mondragon, I. *Macromolecules* **2006**, *39*, 2254–2261.
(10) Dean, J. M.; Lipic, P. M.; Grubbs, R. B.; Cook, R. F.; Bates, F. S. *J. Polym. Sci., Part B: Polym. Phys.* **2001**, *39*, 2996–3010.
(11) Ritzenthaler, S.; Court, F.; David, L.; Girard-Reydet, E.; Leibler, L.; Pascault, J. P. *Macromolecules* **2002**, *35*, 6245–6254.
(12) Girard-Reydet, E.; Pascault, J.; Bonnet, A.; Court, F.; Leibler, L. *Macromol. Symp.* **2003**, *198*, 309–322.
(13) Hermel-Davidock, T. J.; Tang, H. S.; Murray, D. J.; Hahn, S. F. *J. Polym. Sci., Part B: Polym. Phys.* **2007**, *45*, 3338–3348.
(14) Meng, F.; Zheng, S.; Zhang, W.; Li, H.; Liang, Q. *Macromolecules* **2006**, *39*, 711–719.
(15) Meng, F.; Zheng, S.; Li, H.; Liang, Q.; Liu, T. *Macromolecules* **2006**, *39*, 5072–5080.
(16) Meng, F.; Zheng, S.; Liu, T. *Polymer* **2006**, *47*, 7590–7600.
(17) Xu, Z.; Zheng, S. *Macromolecules* **2007**, *40*, 2548–2558.
(18) Fan, W.; Zheng, S. *Polymer* **2008**, *49*, 3157–3167.
(19) Grubbs, R. B.; Broz, M. E.; Dean, J. M.; Bates, F. S. *Macromolecules* **2000**, *33*, 2308–2310.

(20) Grubbs, R. B.; Dean, J. M.; Broz, M. E.; Bates, F. S. *Macromolecules* **2000**, *33*, 9522–9534.
(21) Grubbs, R. B.; Dean, J. M.; Bates, F. S. *Macromolecules* **2001**, *34*, 8593–8595.
(22) Rebizant, V.; Abetz, V.; Tournilhac, F.; Court, F.; Leibler, L. *Macromolecules* **2003**, *36*, 9889–9896.
(23) Rebizant, V.; Venet, A.; Tournilhac, F.; Girard-Reydet, E.; Navarro, C.; Pascault, J.; Leibler, L. *Macromolecules* **2004**, *37*, 8017–8027.
(24) Serrano, E.; Larrañaga, M.; Remiro, P. M.; Mondragon, I.; Carrasco, P. M.; Pomposo, J. A.; Mecerreyes, D. *Macromol. Chem. Phys.* **2004**, *205*, 987–996.
(25) Serrano, E.; Martin, M. D.; Tercjak, A.; Pomposo, J. A.; Mecerreyes, D.; Mondragon, I. *Macromol. Rapid Commun.* **2005**, *26*, 982–985.
(26) Serrano, E.; Tercjak, A.; Kortaberria, G.; Pomposo, J. A.; Mecerreyes, D.; Zafeiropoulos, N. E.; Stamm, M.; Mondragon, I. *Macromolecules* **2006**, *39*, 2254–2261.
(27) Serrano, E.; Tercjak, A.; Ocando, C.; Larrañaga, M.; Parellada, M. D.; Corona-Galván, S.; Mecerreyes, D.; Zafeiropoulos, N. E.; Stamm, M.; Mondragon, I. *Macromol. Chem. Phys.* **2007**, *208*, 2281–2292.
(28) Ocando, C.; Tercjak, A.; Serrano, E.; Ramos, J. A.; Corona-Galván, S.; Parellada, M. D.; Fernández-Berridi, M. J.; Mondragon, I. *Polym. Int.* **2008**, *57*, 1333–1342.
(29) Mijovic, J.; Shen, M.; Sy, J. W.; Mondragon, I. *Macromolecules* **2000**, *33*, 5235–5244.
(30) Guo, Q.; Thomann, R.; Gronski, W.; Thurn-Albrecht, T. *Macromolecules* **2002**, *35*, 3133–3144.
(31) Ritzenthaler, S.; Court, F.; Girard-Reydet, E.; Leibler, L.; Pascault, J. P. *Macromolecules* **2003**, *36*, 118–126.
(32) Larrañaga, M.; Gabilondo, N.; Kortaberria, G.; Serrano, E.; Remiro, P.; Riccardi, C. C.; Mondragon, I. *Polymer* **2005**, *46*, 7082–7093.
(33) Serrano, E.; Martin, M. D.; Tercjak, A.; Pomposo, J. A.; Mecerreyes, D.; Mondragon, I. *Macromol. Rapid Commun.* **2005**, *26*, 982–985.
(34) Meng, F.; Xu, Z.; Zheng, S. *Macromolecules* **2008**, *41*, 1411–1420.
(35) Meng, F.; Yi, F.; Zheng, S. *J. Macromol. Sci., Part B: Phys.* **2008**, *47*, 450.
(36) Liu, J.; Sue, H.; Thompson, Z. J.; Bates, F. S.; Dettloff, M.; Jacob, G.; Verghese, N.; Pham, H. *Macromolecules* **2008**, *41*, 7616–7624.
(37) Fan, W.; Wang, L.; Zheng, S. *Macromolecules* **2009**, *42*, 327–336.
(38) Tang, H. S.; Hermel-Davidock, T. J.; Hahn, S. F.; Murray, D. J.; Cieslinski, R. C.; Verghese, N. E.; Pham, H. Q. *J. Polym. Sci., Part B: Polym. Phys.* **2009**, *47*, 393–406.
(39) Kosonen, H.; Ruokolainen, J.; Nyholm, P.; Ikkala, O. *Polymer* **2001**, *42*, 9481–9486.
(40) Kosonen, H.; Ruokolainen, J.; Torkkeli, M.; Serimaa, R.; Nyholm, P.; Ikkala, O. *Macromol. Chem. Phys.* **2002**, *203*, 388–392.
(41) Sinturel, C.; Vayer, M.; Erre, R.; Amenitsch, H. *Macromolecules* **2007**, *40*, 2532–2538.
(42) Serrano, E.; Gerard, P.; Lortie, F.; Pascault, J.; Portinha, D. *Macromol. Mater. Eng.* **2008**, *293*, 820–827.
(43) Chen, L.; Phillip, W. A.; Cussler, E. L.; Hillmyer, M. A. *J. Am. Chem. Soc.* **2007**, *129*, 13786–13787.
(44) Chen, L.; Hillmyer, M. A. *Macromolecules* **2009**, *42*, 4237–4243.
(45) Phillip, W. A.; Amendt, M.; O'Neill, B.; Chen, L.; Hillmyer, M. A.; Cussler, E. L. *ACS Appl. Mater. Interfaces* **2009**, *1*, 472–480.
(46) Phillip, W. A.; Martono, E.; Chen, L.; Hillmyer, M. A.; Cussler, E. L. *J. Membr. Sci.* **2009**, *337*, 39–46.
(47) Chen, L.; Hallinan, D. T.; Elabd, Y. A.; Hillmyer, M. A. *Macromolecules* **2009**.
(48) Schmidt, S. C.; Hillmyer, M. A. *Macromolecules* **1999**, *32*, 4794–4801.
(49) Wang, Y.; Hillmyer, M. A. *Macromolecules* **2000**, *33*, 7395–7403.
(50) Zalusky, A. S.; Olayo-Valles, R.; Wolf, J. H.; Hillmyer, M. A. *J. Am. Chem. Soc.* **2002**, *124*, 12761–12773.
(51) Hillmyer, M. A.; Bates, F. S. *Macromolecules* **1996**, *29*, 6994–7002.
(52) Hsieh, H. L.; Quirk, R. P. *Anionic Polymerization: Principles and Practical Applications*; Marcel Dekker: New York, 1996; Chapter 10, p 237.
(53) Tobolsky, A. V.; Boudreau, R. J. *J. Polym. Sci.* **1961**, *51*, S53–S56.
(54) Chen, J.; Fetters, L. J. *Polym. Bull.* **1981**, *4*, 275–280.
(55) The gelation time for a DCPD solution in THF (75 wt %) using 0.5 wt % catalyst in the absence of block polymer was about 8.5 min. This difference in gelation time is consistent with the PNS block acting as a multifunctional cross-linking agent, thus decreasing the critical extent of reaction for gelation.
(56) Lichterfeld, F.; Schmeling, T.; Strey, R. *J. Phys. Chem.* **1986**, *90*, 5762–5766.
(57) Teubner, M.; Strey, R. *J. Chem. Phys.* **1987**, *87*, 3195.
(58) Lowell, S. *Introduction to Powder Surface Area*; John Wiley and Sons: New York, 1979; p 199.
(59) Brunauer, S.; Emmett, P. H.; Teller, E. *J. Am. Chem. Soc.* **1938**, *60*, 309–319.
(60) Barrett, E. P.; Joyner, L. G.; Halenda, P. P. *J. Am. Chem. Soc.* **1951**, *73*, 373–380.
(61) Duval, M.; Haida, H.; Lingelser, J. P.; Gallot, Y. *Macromolecules* **1991**, *24*, 6867–6869.
(62) Hiemenz, P. C.; Lodge, T. P. *Polymer Chemistry*, 2nd ed.; CRC Press: Boca Raton, FL, 2007.
(63) Scriven, L. E. *Nature* **1976**, *263*, 123–125.